THE JOURNAL OF BIOLOGICAL CHEMISTRY VOL. 289, NO. 33, pp. 22749–22758, August 15, 2014

Novel $K_v7.1$-Phosphatidylinositol 4,5-Bisphosphate Interaction Sites Uncovered by Charge Neutralization Scanning*

Received for publication, June 16, 2014 Published, JBC Papers in Press, June 19, 2014, DOI 10.1074/jbc.M114.589796

Karina Eckey[‡§¶], Eva Wrobel[‖], Nathalie Strutz-Seebohm[‖], Lutz Pott[**], Nicole Schmitt[‡‡], and Guiscard Seebohm[§¶‖1]

*From the [‡]Department of Biochemistry I–Cation Channel Group, the [§]International Graduate School of Neuroscience, the [¶]Ruhr University Bochum Research School, and the **Institute of Physiology, Ruhr University Bochum, 44801 Bochum, Germany, the [‖]IfGH–Myocellular Electrophysiology, Department of Cardiovascular Medicine, University Hospital of Münster, 48149 Münster, Germany, and the [‡‡]Danish National Research Foundation Centre for Cardiac Arrhythmia, University of Copenhagen, 1165 Copenhagen, Denmark*

Background: Phosphatidylinositol 4,5-bisphosphate (PIP_2) regulates a variety of ion channels including K_v7 channels.
Results: Several $K_v7.1$ mutations impair functional interaction with PIP_2.
Conclusion: PIP_2 interacts with several $K_v7.1$ amino acids, indicating the existence of at least two binding pockets.
Significance: Impaired molecular interaction between mutant $K_v7.1$ and PIP_2 may underlie heart disease.

$K_v7.1$ to $K_v7.5$ α-subunits belong to the family of voltage-gated potassium channels (K_v). Assembled with the β-subunit KCNE1, $K_v7.1$ conducts the slowly activating potassium current I_{Ks}, which is one of the major currents underlying repolarization of the cardiac action potential. A known regulator of K_v7 channels is the lipid phosphatidylinositol 4,5-bisphosphate (PIP_2). PIP_2 increases the macroscopic current amplitude by stabilizing the open conformation of 7.1/KCNE1 channels. However, knowledge about the exact nature of the interaction is incomplete. The aim of this study was the identification of the amino acids responsible for the interaction between $K_v7.1$ and PIP_2. We generated 13 charge neutralizing point mutations at the intracellular membrane border and characterized them electrophysiologically in complex with KCNE1 under the influence of diC_8-PIP_2. Electrophysiological analysis of corresponding long QT syndrome mutants suggested impaired PIP_2 regulation as the cause for channel dysfunction. To clarify the underlying structural mechanism of PIP_2 binding, molecular dynamics simulations of $K_v7.1$/KCNE1 complexes containing two PIP_2 molecules in each subunit at specific sites were performed. Here, we identified a subset of nine residues participating in the interaction of PIP_2 and $K_v7.1$/KCNE1. These residues may form at least two binding pockets per subunit, leading to the stabilization of channel conformations upon PIP_2 binding.

The voltage-gated potassium channel $K_v7.1$ (also called KCNQ1 and K_vLQT1) is one of five members of the K_v7 subfamily. It is foremost expressed in the heart and epithelial tissues of many organs (1, 2). Although $K_v7.1$ can assemble with all five members of the KCNE β-subunit family, its interaction with KCNE1 (also called minK or IsK) is best described (1, 3–7). The noninactivating $K_v7.1$/KCNE1 channel complex shows slow activation and deactivation kinetics (1, 4, 8, 9). These channels mediate the slowly activating cardiac potassium current I_{Ks} (1, 3), which contributes to the repolarization of myocyte membranes during phase 3 of the cardiac action potential (10, 11). Many mutations in $K_v7.1$- and KCNE1-encoding genes have been reported to result in loss of function and to cause long QT syndrome (LQTS),[2] which is associated with cardiac arrhythmia, syncope, and sudden cardiac death (12–18).

All K_v7 channels are inhibited after stimulation of G_q- or G_{11}-protein-coupled receptors (19–22). This is assumed to be primarily due to depletion of the plasma membrane lipid phosphatidylinositol 4,5-bisphosphate (PIP_2) upon activation of phospholipase C (23–25). PIP_2 is important for the function of many proteins, including trafficking molecules such as small GTPases (26, 27) and cytoskeletal proteins (28, 29), as well as transporters and ion channels (30).

Among the ion channels regulated by PIP_2 are transient receptor potential channels, (32), inward-rectifier potassium (K_{ir}) channels (33), and voltage-gated potassium channels such as $K_v7.1$. The lipid presumably exerts its effect on the latter by stabilizing the open channel conformation, thereby slowing the deactivation kinetics and shifting the activation curve to more negative potentials (34).

To date, the interaction has been localized to the C terminus of $K_v7.1$, in which four amino acids have been identified to interact with PIP_2 (35). However, it is not known whether the interaction site is confined to these amino acids. The aim of the present study, therefore, was the identification of residues within $K_v7.1$ responsible for the interaction with PIP_2. Our experiments were based on the assumption that direct interaction is caused by electrostatic forces between negatively

* This work was supported by Deutsche Forschungsgemeinschaft Grant 1077/3-1 and by student grants of the International Graduate School of Neuroscience (Ruhr University Bochum) and the Ruhr University Bochum Research School (to K. E.).

[1] To whom correspondence should be addressed: IfGH–Myocellular Electrophysiology, Dept. of Cardiovascular Medicine, University Hospital of Münster, 48149 Münster, Germany. Tel.: 49-251-8358355; E-mail: guiscard.seebohm@ukmuenster.de.

[2] The abbreviations used are: LQTS, long QT syndrome; PIP_2, phosphatidylinositol 4,5-bisphosphate; K_{ir}, inward rectifier potassium channel; PtdIns, phosphatidylinositol; RMSD, root mean square deviation.

charged PIP_2 head groups and positively charged amino acid residues. Hence, we generated neutralizing mutants of 13 positively charged amino acids. These were coexpressed with KCNE1 in *Xenopus laevis* oocytes to form slowly activating (I_{Ks}) channels. Effects of injected diC_8-PIP_2 on wild type and mutant channels was investigated by means of the two-electrode voltage-clamp. Included in the charge neutralization scan were the residues identified by Thomas *et al.* (35). Nine of the thirteen amino acids proved positive for a functional interaction with the lipid. Five of these had been identified previously as LQTS mutants. Electrophysiological analysis revealed an impaired PIP_2 interaction with two of these. Two regions containing examined amino acids bound PIP_2 and other lipids in lipid binding assays. To gain insight into the underlying structural mechanisms, we conducted molecular dynamics simulations of $K_v7.1$ tetramers in complex with four KCNE1 β-subunits, both with and without PIP_2 molecules. The results implied that binding of PIP_2 to at least eight specific binding sites causes the stabilization of open and closed channel conformations.

EXPERIMENTAL PROCEDURES

Molecular Biology—The molecular biological procedures were previously described (36). A mutant channel based on human $K_v7.1$ (GenBank™ accession number NM_000218, isoform 0; the N terminus is truncated compared with isoform 1) in which all cysteines were mutated to alanines ($K_v7.1$ clone without cysteines, here called $K_v7.1$ −cys) was described before and kindly provided by G. N. Tseng (Virginia Commonwealth University, Richmond, VA) (37). The clone was subcloned into the oocyte expression vector pSGEM. Further, human $K_v7.1$ wild type, isoform 1 was subcloned into pXOOM. Human KCNE1 (GenBank™ accession number NM_000219) was subcloned into pSP64. The $K_v7.1$ mutations H126C, R181C, K183C, R190C, R192C, R195C, K196C, R249C, R259C, K354C, K358C, R360C, and K362C were introduced into the $K_v7.1$ −cys clone, the $K_v7.1$ mutations R190L, R192H, R195W, K354R, R360M, R360T, and K362R were introduced into the $K_v7.1$ WT clone by site-directed mutagenesis (Agilent Technologies, Santa Clara, CA). All constructs were confirmed by automated DNA sequencing. The plasmids were linearized using XbaI ($K_v7.1$ −cys), NheI ($K_v7.1$ WT), and EcoRI (KCNE1). *In vitro* synthesis of cRNA was performed using the *T7* ($K_v7.1$) or *SP6* (KCNE1) mMessage mMachine kit (Ambion, Austin, TX) according to the manufacturer's instructions.

Electrophysiology—X. laevis oocytes were harvested in accordance with German laws as previously described (36). Ovarian lobes from tricaine-anesthetized *X. laevis* were digested with collagenase (Type II, Worthington, 1 mg/ml in calcium-free Barth's solution) for ~120 min. Stage V and VI oocytes were injected with ~20 nl of cRNA solution. Oocytes were injected with 2.5 ng of $K_v7.1$ WT or mutant cRNA and 2.5 ng of KCNE1 WT cRNA. The oocytes were stored for 3–4 days at ~18 °C in Barth's solution containing 88 mmol/liter NaCl, 1.1 mmol/liter KCl, 2.4 mmol/liter $NaHCO_3$, 0.3 mmol/liter $Ca(NO_3)_2$, 0.3 mmol/liter $CaCl_2$, 0.8 mmol/liter $MgSO_4$, 15 mmol/liter HEPES-NaOH, 31 mg/liter penicillin-G, 50 mg/liter gentamicin, 20 mg/liter streptomycin sulfate, and 80 mg/liter theophylline, pH 7.6. Two-electrode voltage-clamp recordings were performed at ~22 °C using a Turbo Tec-10CX amplifier (NPI, Tamm, Germany) equipped with a Digidata 1322A AD/DA interface and pCLAMP 9.0 software (Axon Instruments Inc./Molecular Devices, Sunnyvale, CA). The data were analyzed with Clampfit 9.0 (Axon Instruments Inc.), Prism 4.00 (GraphPad Software, La Jolla, CA), and QtiPlot (Ion Vasilief, Craiova, Romania). Recording pipettes were filled with 3 M KCl and had resistances of 0.4–1 MΩ. Channel currents were recorded in ND96 recording solution containing 96 mmol/liter NaCl, 4 mmol/liter KCl, 1.8 mmol/liter $MgCl_2$, 1.0 mmol/liter $CaCl_2$, and 5 mmol/liter HEPES, pH 7.6. Some oocytes were injected with 13.8 ng (−cys mutants) or 27.6 ng (LQTS mutants and comparison WT/−cys) of diC_8-PIP_2 (P-4508; Mobitec, Göttingen, Germany) at least 30 min prior to the recordings. All other reagents were purchased from Sigma-Aldrich.

Lipid Binding Assay—The assay was recently described in detail (31). In brief, PIP Strips from Molecular Probes were used (P23750). The peptides were FITC-labeled and had the following amino acid sequences: Q1-S2/S3, (FITC)-CRSKYVGLWGRLRFARK; Q1-S4/S5, (FITC)-GTWRLLGSVVFIHRQEL; and Q1-S6, (FITC)-GSGFALKVQQKQRQKHF.

PIP Strips membranes were blocked with TBS-T containing 10 mmol/liter Tris-HCl, pH 8.0, 150 mmol/liter NaCl (containing 0.1% (v/v) Tween 20 detergent) + 3% fatty acid-free BSA and gently agitated for 1 h at room temperature protected from light. The peptides (50 μg/ml) were each solved in TBS-T + 3% fatty acid-free BSA and incubated on the membranes for 1 h at room temperature protected from light, using gentle agitation. The membranes were then washed three times for 10 min each with TBS-T + 3% fatty acid-free BSA, protected from light, and gently agitated. Peptide binding was detected by analysis of fluorescence signal.

Molecular Dynamics Simulations—The $K_v7.1$/KCNE1 structural models from Kang *et al.* (38) were used. Eight PIP_2 molecules were introduced in proximity to the eight residue clusters identified by electrophysiology. Structures with and without PIP_2 were inserted into a membrane (composition PEA/PSE/PCH = 1/1/1) and incorporated into a simulation box filled with NaCl-H_2O (0.9%). All-atoms-mobile simulations were performed to reach stable conformations using YASARA Structure version 10.1 (YASARA Biosciences GmbH, Vienna, Austria) as previously described (39).

Data Analysis—Mean current-voltage curves were analyzed using the Boltzmann equation multiplied with the driving force, considering increased current amplitudes caused by increased applied voltages,

$$I(V) = \left(B + \frac{A - B}{1 + e^{\frac{V_{1/2} - V}{\tau}}} \right) \cdot (V - E_K) \qquad \text{(Eq. 1)}$$

where I is the current amplitude, V is the applied voltage, E_K is the potassium equilibrium potential, $V_{½}$ is the half-maximal activation voltage, τ is the time constant, and A and B are the maximal and minimal current amplitudes, respectively.

The variation of structures during the molecular dynamics simulations is presented as the root mean square deviation, which is a measure of the deviation of the atom positions compared with the first structure,

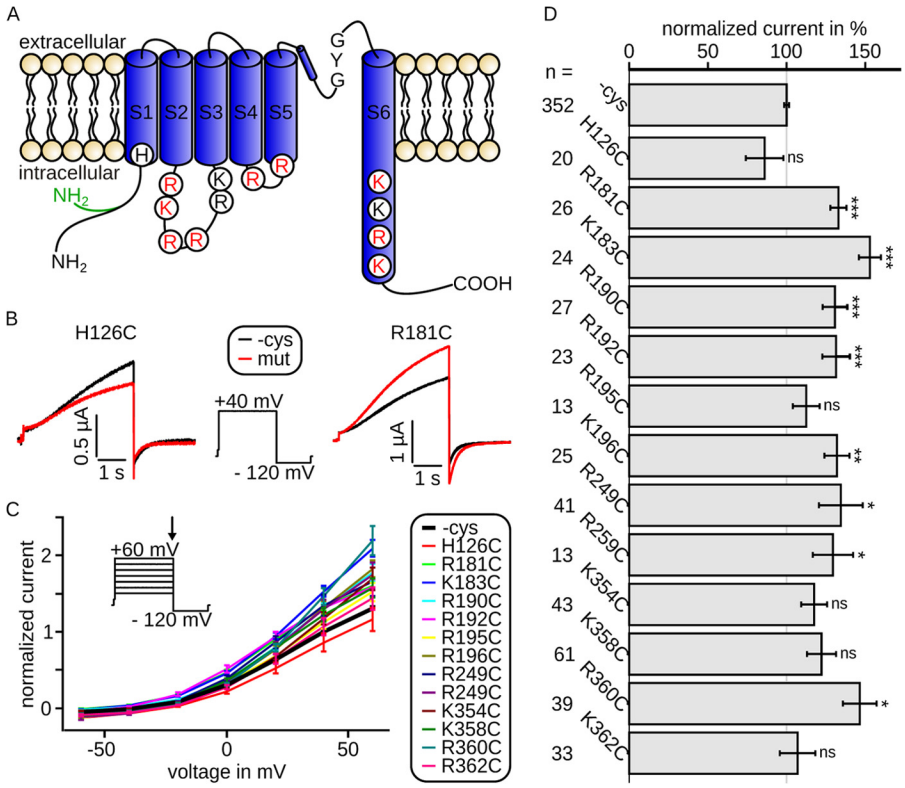

FIGURE 1. **Intracellularly located mutations modulate $K_v7.1$/KCNE1 channel currents.** Currents were recorded 3 days after injection. *A*, topology model of $K_v7.1$, showing all six transmembrane segments S1–S6 with pore loop and selectivity filter sequence GYG. Shown are all amino acids included in this study. *Red*, necessary for interaction with PIP_2; *black*, not relevant for interaction with PIP_2 (according to our electrophysiological data; see Fig. 2). The cysteine-free clone used in this study is based on isoform 0, whose N terminus is 95 amino acids shorter than isoform 1 and in which the first 11 amino acids are altered (*green*). *B*, representative current traces and voltage protocol with steps from −100 to 40 mV to −120 mV. Current of mutant H126C (*red*) was slightly decreased compared with wild type (*black*), whereas the current of mutant R181C was increased. *C*, mean data ± S.E. of current-voltage relationships between wild type (emphasized) and mutants are similar. The *arrow* in voltage-step protocol marks the time point of analysis. *D*, currents at 40 mV were normalized to the corresponding wild type. The mean data ± S.E. (all wild type recordings averaged) show significantly increased (R181C, K183C, R190C, R192C, K196C, R249C, R259C, and R360C) or unchanged (H126C, R195C, K354C, K358C, and K362C) current amplitudes. *n*, number of oocytes. *Asterisks* indicate significance: ***, $p < 0.001$; **, $p < 0.01$; *, $p < 0.05$; *ns*, not significant.

$$\mathrm{RMSD}(t_1,t_2) = \sqrt{\frac{1}{M}\sum_{i=1}^{N} m_i \cdot (\vec{r}_i(t_1) - \vec{r}_i(t_2))^2} \qquad \text{(Eq. 2)}$$

where $t_1 = 0$, N is the number of atoms, $\vec{r}_i$ is the position of atom i at time t, m_i is the atom mass, and M is the sum of the atom masses.

RESULTS

Electrophysiological Examination of $K_v7.1$ Mutants—Wild type (cysteine-free $K_v7.1$, −cys) or mutated $K_v7.1$/KCNE1 channels were expressed in *X. laevis* oocytes. The examined mutations are located in transmembrane segment S1 (H126C), the intracellular linker between S2 and S3 (R181C, K183C, R190C, R192C, R195C, and K196C), the intracellular linker between S4 and S5 (R249C and R259C), and the intracellular extension of helix S6 (K354C, K358C, R360C, and K362C; Fig. 1*A*). All channels yielded characteristic, noninactivating, slowly activating and deactivating, voltage-gated potassium currents (Fig. 1*B*). Current-voltage relationships (Fig. 1*C*) showed WT (−cys) or mutant channel activation upon depolarization to approximately −30 mV. The shapes of the curves and hence kinetic parameters appeared nearly unchanged, but some mutations led to significantly increased current amplitudes compared with WT (−cys) currents (Fig. 1, *B*, *red curves*, and *D*).

Because oocyte batches may vary in their endogenous PIP_2 levels and hence binding sites may be occupied to different extents, we included only those batches in which increased WT currents were observed after PIP_2 application. In these batches, currents of the mutants were increased, decreased, or unchanged (Fig. 2*A*). To discover different properties upon diC_8-PIP_2 application, we analyzed current amplitudes. The amplitudes at 40 mV were normalized to the respective current without the PIP_2 analog diC_8-PIP_2 of each individual batch (Fig. 2*B*). diC_8-PIP_2 significantly increased the WT (−cys) current amplitude to ~160% on average, as well as the amplitudes of four mutants shown in *gray* (H126C, R195C, K196C, and K358C). Supposedly, the stimulation indicates that diC_8-PIP_2 was able to stabilize the open channel conformation of these mutants. Four mutants showed reduced stimulation (marked in *blue*; K183C, R190C, R249C, and K354C) to values between 120 and 150%. In contrast, currents of mutants shown in *red* (R181C, R192C, R259C, R360C, and K362C) were either not affected or even significantly decreased by up to 25% upon diC_8-PIP_2 injection, indicating an impaired functional interaction with PIP_2. Further analysis of the diC_8-PIP_2 effects on

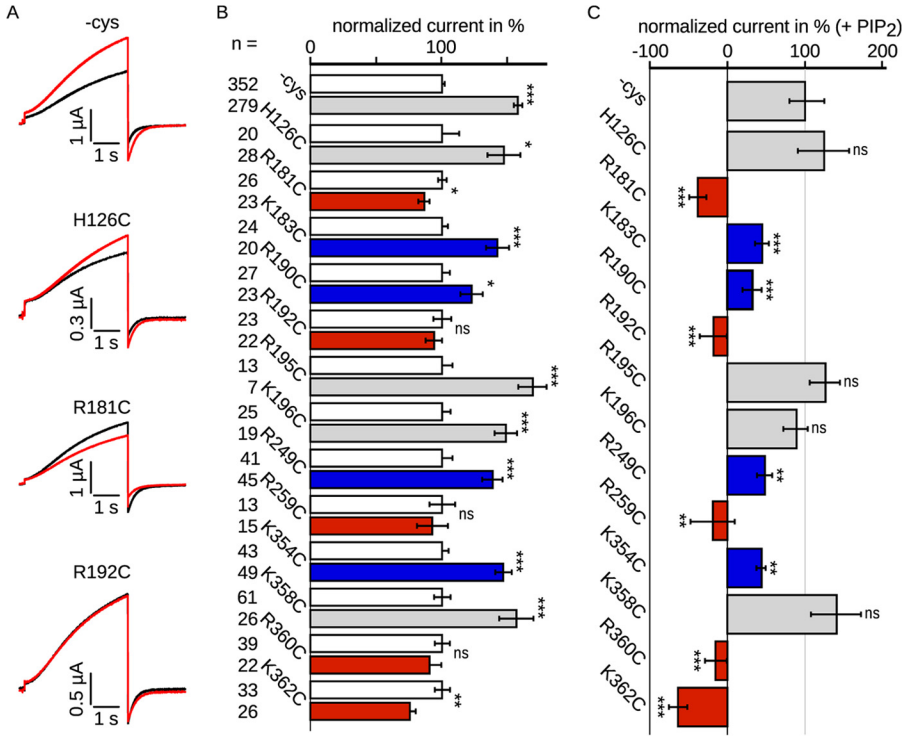

FIGURE 2. **$K_v7.1$/KCNE1 channel currents were changed in oocytes upon injection of the water soluble PIP_2 analog diC_8-PIP_2.** Currents were recorded 3–4 days after injection. diC_8-PIP_2 was injected at least 30 min prior to the recordings. *A*, representative current traces recorded with the voltage protocol shown in Fig. 1*B*. *Black*, without diC_8-PIP_2; *red*, with diC_8-PIP_2. Currents were increased (wild type and H126C), decreased (R181C), or unchanged (R192C) by diC_8-PIP_2. *B*, current amplitudes recorded in the presence of diC_8-PIP_2 were normalized to the corresponding currents without diC_8-PIP_2. The mean data ± S.E. at 40 mV show changes in currents amplitude by diC_8-PIP_2. Currents of wild type (all recordings averaged), H126C, K183C, R190C, R195C, K196C, R249C, K354C, and K358C were increased by diC_8-PIP_2. Currents of R181C, R192C, R259C, R360C, and K362C were unchanged or decreased upon diC_8-PIP_2 application. *C*, results with diC_8-PIP_2 were scaled and normalized to the wild type amplitude of the individual batch of oocytes also with diC_8-PIP_2. Hence, the value of 100% represents the increase of current amplitude for WT channels by diC_8-PIP_2, a value of 0 reflects no change in current amplitude by diC_8-PIP_2 at all, and values below 0 show decreased current amplitudes. Mutants equally increased as wild type (H126C, R195C, K196C, and K358C) are colored in *gray*. Mutants with reduced diC_8-PIP_2 stimulation compared with wild type (K183C, R190C, R249C, and K354C) are colored in *blue*, and those mutants whose function is completely inhibited upon diC_8-PIP_2 application (R191C, R192C, R259C, R360C, and K362C) are colored in *red*. *n*, number of oocytes. *Asterisks* indicate significance: ***, $p < 0.001$; **, $p < 0.01$; *, $p < 0.05$; *ns*, not significant.

mutant channel currents compared with wild type emphasized these differences (Fig. 2*C*). Here, current amplitudes were normalized to the WT (−cys) current with diC_8-PIP_2 of each individual batch. This analysis indicated no significant differences between current amplitudes of wild type and mutants shown in *gray*, suggesting that these residues do not play a significant role in the protein-lipid interaction. In contrast, current amplitudes of mutants depicted in *blue* were stimulated to a lesser extent compared with WT channels, implying an involvement in the interaction. Intriguingly, currents carried by several mutants shown in *red* were unchanged or reduced by diC_8-PIP_2 injection, suggesting an important role for these residues in PIP_2 coordination.

Next we analyzed current-voltage relationships of the neutralizing mutants after injection of diC_8-PIP_2. To examine differences in voltage dependence of activation caused by diC_8-PIP_2, we fit our data according to the Boltzmann equation multiplied by the driving force (representative fits in Fig. 3*A*). Analysis of the half-maximal activation voltage $V_{½}$ showed that the values of the various mutants were distributed between −20 and 10 mV compared with −4 mV of the WT (−cys) (Fig. 3*B*). The voltage dependences of WT (−cys) and mutants R181C, R190C, R249C, R259C, and K358C were unchanged by diC_8-PIP_2. The voltage dependences of mutants R192C, K354C, and R360C were shifted by diC_8-PIP_2 to more negative potentials. Half-maximal activation voltages of mutants H126C, K183C, R195C, K196, and K362C were shifted to more positive potentials. However, significances could not be determined. Comparison between half-maximal activation voltage upon diC_8-PIP_2 injection and current-amplitude changes revealed no correlation (Fig. 3*C*).

As a control, we compared the effect of diC_8-PIP_2 on $K_v7.1$ WT and −cys (Fig. 4*A*). Both current amplitudes were augmented, however, with −cys augmented to a slightly but significantly lesser extent.

Notably, there are known LQTS mutants at amino acid positions 190, 192, 195, 354, 360, and 362. Because we could observe an impaired diC_8-PIP_2 regulation when neutralizing these residues, we hypothesized that the impaired regulation is the underlying cause for channel dysfunction. Therefore, we also investigated these mutations electrophysiologically under the influence of diC_8-PIP_2 (Fig. 4*B*). Indeed, mutations R190L, R192H, and R195W showed less increased current amplitudes. Mutations K354R and K362R showed even enhanced current amplitude increases (not significantly and significantly, respectively). Mutations R360T and R360M did not yield functional currents (data not shown).

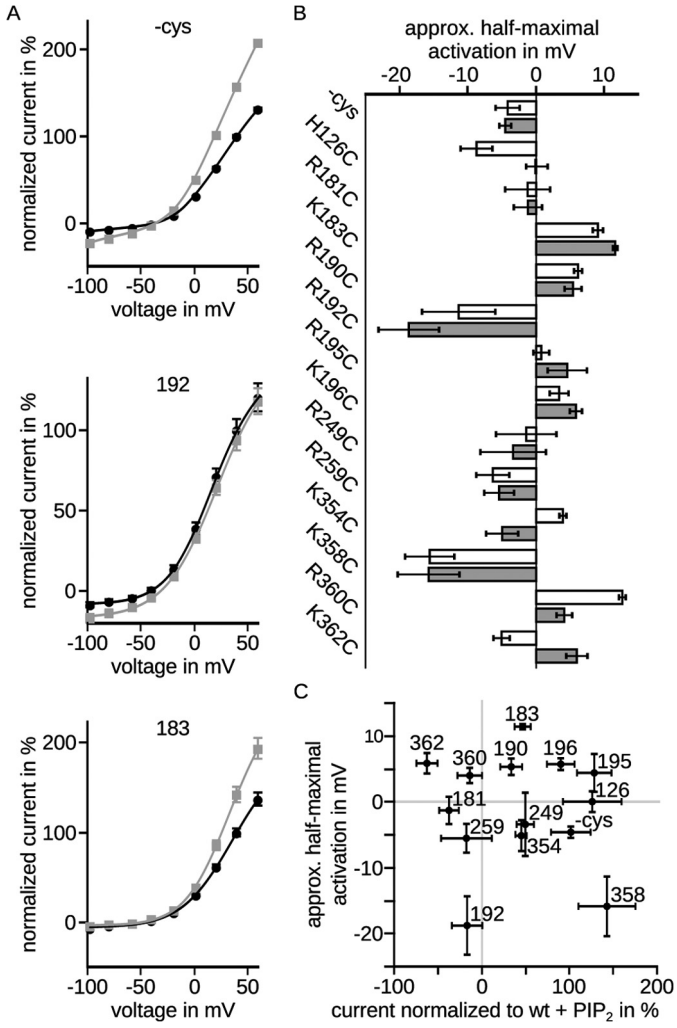

FIGURE 3. **Conductivity-voltage relationships were differently affected by diC_8-PIP_2.** Currents were recorded 3 days after injection. diC_8-PIP_2 was injected at least 30 min prior to the recordings. *A*, channel conductivity was calculated from current-voltage relationships obtained by the voltage protocol shown in Fig. 1*B*. The mean data ± S.E. were fit according to the Boltzmann equation multiplied with the driving force. *Black*, without diC_8-PIP_2; *gray*, with diC_8-PIP_2. Representative fits showed that saturation was not reached. *B*, half-maximal activation voltages ± fit error were unchanged (WT, R181C, R190C, R249C, R259C, and K358C) or shifted to positive (H126C, K183C, R195C, K196C, and K362C) or negative potentials (R192C, K354C, and R360C) by diC_8-PIP_2. *White*, without diC_8-PIP_2; *gray*, with diC_8-PIP_2. Significance could not be determined. *C*, half-maximal activation voltage ± fit error is compared with normalized current amplitudes ± S.E. shown in Fig. 2*C*. Clearly, no correlation between half-maximal activation voltage and normalized current amplitudes could be detected.

Lipid Binding Assay—The S2-S3 linker, the S4-S5 linker, and the C-terminal part of S6, all containing the examined amino acids, were subjected to lipid binding assays (Fig. 4*C*). Both the S2-S3 linker and S6 were shown to bind to all phosphatidylinositol (PtdIns) phospho derivatives, including PIP_2. Additionally, the S6 fragment was positive for phosphatidyl serine binding. The S4-S5 linker did not bind to any of the tested lipids.

Molecular Dynamics Simulation—We based molecular dynamics simulations on $K_v7.1$/KCNE1 models (4:4 relation because of the ongoing discussion on stoichiometry (40)) in a closed and an open conformation as described by Kang *et al.* (38) and introduced eight PIP_2 molecules into the models. Conventional molecular dynamics simulations on channels in a membranous environment were performed until stable structures were reached. The last nanosecond of each simulation was averaged (Fig. 5*A*, *cyan* without PIP_2 and *yellow* with PIP_2) and compared with the starting structure (Fig. 5*A*, *green*). In the open conformation, differences between the starting structure and the average without the lipid were slightly larger than the differences between the starting structure and the average with PIP_2. In the closed conformation, the structural differences without PIP_2 were much larger than in presence of PIP_2.

Root mean square deviation (RMSD) analysis, which indicates the structural variation over time, showed that all structures were in equilibrium for at least the last nanosecond of simulation (Fig. 5*B*). In equilibrium, the RMSD of all simulations were ~4 Å, except for the closed conformation with PIP_2 with an RMSD of ~3 Å, agreeing with the direct visual comparison of the structures. The RMSD values of the simulations with and without PIP_2 in the open conformation (Fig. 5*C*, *green* and *blue*) were almost identical, whereas there was a large difference of ~1 Å in the closed conformation (Fig. 5*C*, *black* and *violet*). Residue-resolved RMSD values were averaged over time and all four subunits (Fig. 5*C*). These values confined these results to the pore region, beginning with the S4-S5 linker, because the voltage sensor itself is much more flexible. Both regions seemed more flexible when all four subunits were averaged, although this was not the case for each individual subunit (data not shown). The results were confirmed by the averaged RMSD of the S4-S5 linker (residues 249–261) and pore helix to the upper part of helix S6 region (residues 305–343; Fig. 4*D*). RMSD values without PIP_2 were enlarged by factors of ~1.8 and 1.3 (linker) and 1.5 and 1.2 (S6) in the closed and open conformation, respectively.

In addition, both PIP_2-free structures were distorted. That is, α-helices were bent or in part degraded, hinting at a destabilization of the channel in the absence of PIP_2. Recently, Hansen *et al.* (41) and Whorton and MacKinnon (42) demonstrated electrostatic interactions as the basis for PIP_2 binding in K_{ir} channels, underscoring our assumption. Our results agreed with these data, because some identified residues surrounded the PIP_2 head groups (Fig. 5*E*).

DISCUSSION

PIP_2 is a known regulator of diverse ion channels and transporters (30). Recently, two crystal structures of ion channels in complex with PIP_2 have been resolved. Key to the interaction of channels with PIP_2 are positively charged residues that enable electrostatic interactions with the negatively charged phosphates of PIP_2 (41, 42). There are several charged residues at the predicted membrane border of the inner membrane leaflet, which potentially represent PIP_2 interaction sites. In this study, we scanned for amino acids in $K_v7.1$ that functionally interact and potentially bind to PIP_2. Wild type current amplitudes were up-regulated by PIP_2 to different extents, probably depending on the amount of endogenous PIP_2 and whether its concentration was saturating.

First of all, we observed some mutants (R181C, K183C, R190C, R192C, K196C, R249C, R259C, and R360C) with increased current amplitudes compared with WT channels without the influence of diC_8-PIP_2. Second, we identified resi-

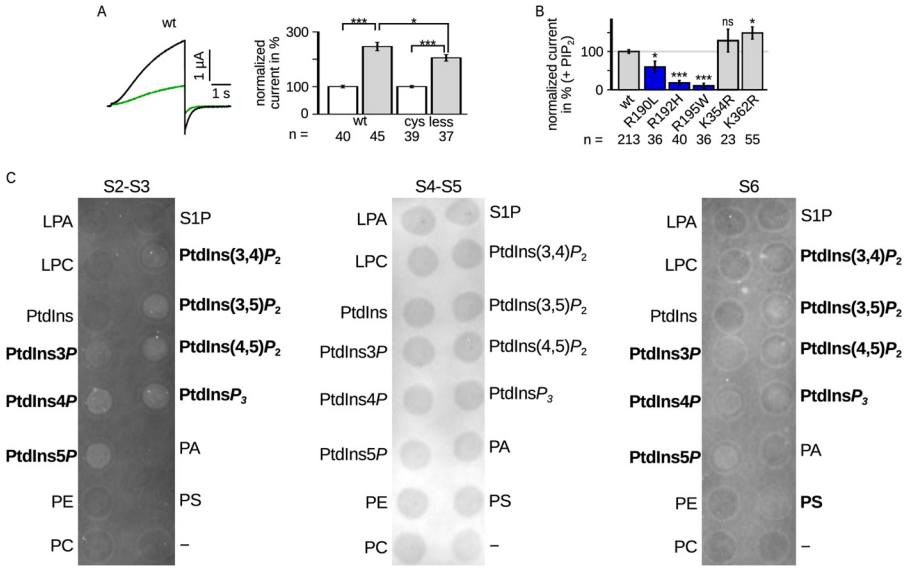

FIGURE 4. *A*, LQTS mutants impaired PIP_2 regulation. Comparison of $K_v7.1$ −cys and WT. *Left panel*, representative current amplitude (*black*, WT; *green*, −cys). *Right panel*, current amplitudes recorded in the presence of diC_8-PIP_2 were normalized to the corresponding currents without diC_8-PIP_2. The mean data ± S.E. at 40 mV showed similar changes in currents amplitude. *B*, LQTS mutants were measured with and without diC_8-PIP_2. The results with diC_8-PIP_2 were scaled and normalized to the wild type amplitude of the individual batch of oocytes also with diC_8-PIP_2. Three mutants were lesser increased (*blue*). *n*, number of oocytes. *Asterisks* indicate significance: ***, $p < 0.001$; **, $p < 0.01$; *, $p < 0.05$; ns, not significant. *C*, the S2-S3 linker and S6 fragment bound PIP_2 *in vitro*. Representative lipid binding assays of the S2-S3 linker (CRSKYVGLWGRLRFARK), S4-S5 linker (GTWRLLGSVVFIHRQEL), and part of S6 (ALKVQQKQRQKHFNR). Binding of the S2-S3 linker and S6 fragment was demonstrated with PtdIns3*P*, PtdIns4*P*, PtdIns5*P*, PtdIns(3,4)P_2, PtdIns(3,5)P_2, PtdIns(4,5)P_2, and PtdInsP_3. S6 also bound to PS. No binding was observed for the S4-S5 linker. Positive results are emphasized. *LPA*, lysophosphatidic acid; *LPC*, lysophosphatidylcholine; *PtdInsP*, phosphatidylinositol phosphate; *PE*, phosphatidylethanolamine; *PC*, phosphatidylcholine; *S1P*, sphingosine 1-phosphate; *PtdInsP$_2$*, phosphatidylinositol bisphosphate; *PtdInsP$_3$*, phosphatidylinositol trisphosphate; *PA*, phosphatidic acid; *PS*, phosphatidyl serine.

dues Lys-183, Arg-190, Arg-249, and Lys-354 to be necessary for PIP_2 regulation, because their currents were increased by diC_8-PIP_2 to a lesser extent than WT currents. Finally, amino acids Arg-181, Arg-192, Arg-259, Arg-360, and Lys-362 seemed even more important because diC_8-PIP_2 failed to stimulate channel currents or even inhibited function. In the latter case, binding of PIP_2 to the mutants may be so unfavorable that the equilibrium shifts toward the closed instead of the open state. Interestingly, these mutants were the same as those that showed increased current amplitudes compared with WT currents with only three exceptions (K196C, K354C, and K362C). This suggests that endogenous PIP_2 significantly influences current amplitudes.

To determine whether changed effects on current amplitudes of the neutralizing mutants can be explained by differences in channel kinetics, we analyzed the half-maximal activation voltage of WT and mutant channels. First of all, half-maximal activation voltages of many mutants differ largely from the wild type, which might be influenced by changed interaction with endogenous PIP_2. Half-maximal activation voltage of WT was unchanged by application of diC_8-PIP_2. However, half-maximal activation voltages of several mutants were either shifted to more positive or negative potentials. Nevertheless, these $V_{½}$ shifts do not correlate with the current-amplitude change upon diC_8-PIP_2 application. One factor may be weak analysis of the $V_{½}$ values, because Boltzmann fits were difficult to obtain, since conductivity-voltage relationships did not reach saturation (43), compromising detailed interpretation. The lack of $V_{½}$-I_{PIP_2} correlation suggests either complete or partial independence and too complex interaction of PIP_2 molecules to be analyzed by the techniques used here.

Mutations of several amino acids that we identified as PIP_2 interaction sites have been reported to be associated with LQTS (R190L, R190W, and R190Q; R192H and R192P; R195W; R259H, R259L, and R259C; K354R; R360G, R360T, and R360M; and K362R) (51–58). It is plausible that disturbed PIP_2 interaction may contribute to an impaired channel function responsible for LQTS. For all of these residues, except for Arg-195, we demonstrated that the current amplitude was not changed by diC_8-PIP_2 or significantly less increased than WT current amplitude, further supporting the notion that impaired PIP_2 binding, and hence regulation is involved in the pathogenesis of LQTS. To test this hypothesis, we investigated some of the mentioned mutations. Indeed, in mutants R190L, R192H, R195W, and R259C, regulation by PIP_2 was disturbed, corroborating our assumption. It is noteworthy that also R195W was up-regulated to a lesser extent, although we could not see a difference between R195C and the wild type. Therefore, it is presumable that not the neutralization of the arginine is responsible for the disturbed regulation but rather conformational changes introduced by tryptophan. Analysis of both conserved mutations K354R and K362R, on the other hand, revealed preserved PIP_2 regulation, which can be easily explained by the conservation of positive charges. Therefore, a disturbed PIP_2 regulation cannot explain channel dysfunction and LQTS development in these cases.

To date, PIP_2 binding sites have been identified mainly in the C terminus of ion channels. That is, residues in the C terminus of various inward rectifier potassium (K_{ir}) channels have been shown to participate in PIP_2 binding (33, 29, 44–48). Recently, the binding site in K_{ir} channels has been located to the interface between transmembrane domain and C terminus (41, 42). Also,

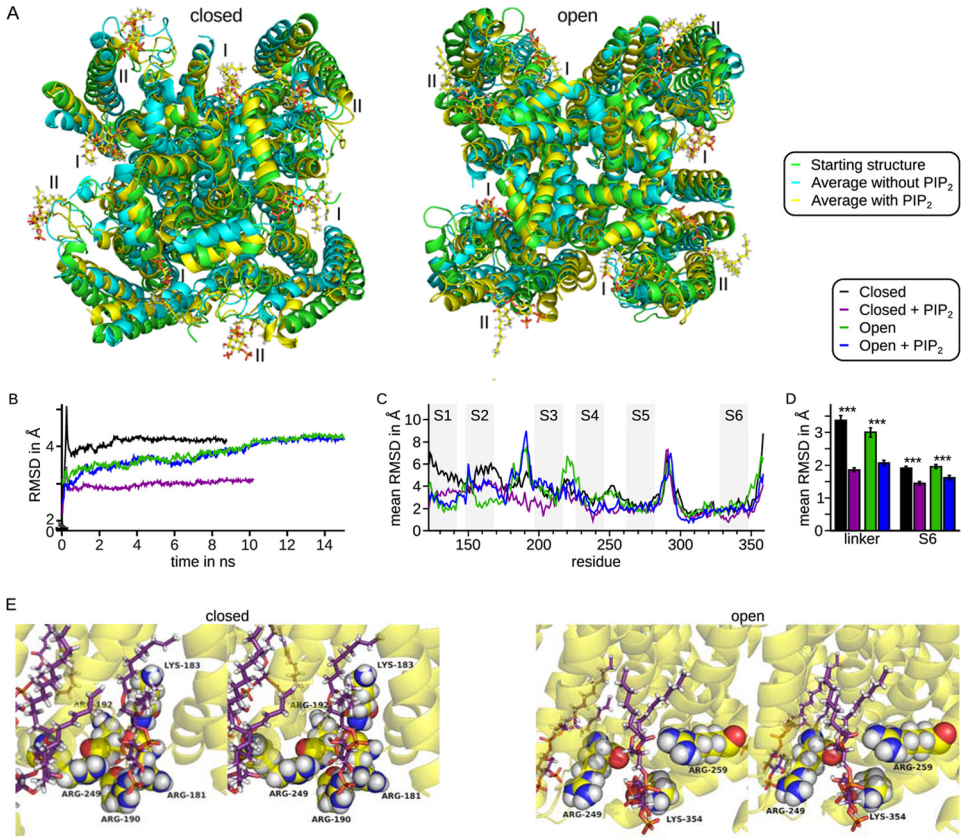

FIGURE 5. **Molecular dynamics simulations of $K_v7.1$/KCNE1 in closed and open conformations showed stabilization of the structures by PIP_2.** *I*, assumed inner binding site; *II*, assumed outer binding site. Four $K_v7.1$ subunits in complex with four KCNE1 subunits were incorporated into a membrane and NaCl-H_2O. *A*, first structures (*green*) and mean structures of the last ns of the closed (*left panel*) and open (*right panel*) conformation without (*cyan*) and with (*yellow*) PIP_2, shown from the intracellular side. *Yellow*, carbon; *white*, hydrogen; *red*, oxygen; *orange*: phosphor. *B*, RMSD during the simulations show that a stable conformation was reached. *C*, residue-resolved mean RMSD, averaged over time and subunits. Numbering of residues was in accordance with $K_v7.1$ variant 1 (GenBank™ accession number NM_000218). *Gray rectangles* show the approximate transmembrane segments. Large variations were seen in the voltage sensor. Small variations were seen in the S4-S5 linker and helix S6. *D*, mean RMSD (time, residue, and subunit) for the S4-S5 linker (residues 249–261) and pore helix to helix S6 (residues 305–343). The mean RMSD were increased in the absence of PIP_2 in both closed and open conformation. *Asterisks* indicate significance: ***, $p < 0.001$. *E*, stereo view of one PIP_2 molecule (*sticks*) surrounded by several positively charged residues (*spheres*) in the closed (*left panel*) and open (*right panel*) conformation in the averaged structure. *Yellow*, $K_v7.1$ backbone and carbon; *violet*, carbon of PIP_2; *white*, hydrogen; *red*, oxygen; *blue*, nitrogen; *orange*, phosphor.

a cluster of basic amino acids in the C terminus of $K_v7.2$ and $K_v7.3$ has been demonstrated as a PIP_2 binding site (49). Moreover, the C-terminal residues Arg-539 and Arg-555 within $K_v7.1$ have been shown to participate in the interaction with PIP_2 (50). The amino acids identified here are located in the C-terminal portion of helix S6 beneath the membrane (Lys-354, Arg-360, and Lys-362) but also in the intracellular linkers between S2 and S3 (Arg-181, Lys-183, Arg-190, and Arg-192), as well as between S4 and S5 (Arg-249 and Arg-259; Fig. 2*C*). Unspecific binding to PtdIns was shown for both the S2-S3 linker and the C-terminal fragment of S6. This is in contrast to an earlier study by Thomas *et al.* (35), who reported that PIP_2 binds exclusively in the C terminus, because they did not observe lipid binding of the C-terminally truncated protein in lipid binding assays. A possible explanation for this conflict might be an incorrect folding of the truncated protein. However, Zaydman *et al.* (59) analyzed the same regions as in this study and also concluded that these regions form PIP_2 binding sites. In contrast to the electrophysiological data, the S4-S5 linker did not bind to any of the tested lipids. A possible explanation is that the investigated region is not sufficient for PIP_2 binding but requires further protein parts, for example Arg-243, which was already demonstrated to reduce PIP_2 affinity (50). However, amino acids Arg-249 and Arg-259 may affect PIP_2 regulation allosterically.

Residues outside of the C terminus have been detected before, for instance in the N terminus of K_{ir} channels (42, 46, 48) and at the end of S4 in $K_v7.1$ (50). Thus, it is possible that all basic residues in a certain distance to the membrane mediate interaction with PIP_2 without forming a specific binding site. However, in our model obtained from the molecular dynamics simulations, the identified residues were clustered and might form distinct binding pockets because of their tertiary structure. The PIP_2 molecules were in direct contact with most identified residues. These residues might form two binding pockets per subunit together with noncharged residues or the protein backbone. The positions of these proposed binding sites are indicated in Fig. 6. Binding site I in Fig. 6 seemed to be close to the pore domain, which is in line with recent work by Hansen *et al.* (41), as well as Whorton and MacKinnon (42) showing PIP_2 molecules in this region in K_{ir} channel crystal structures. Our results suggest a second binding site in each subunit located further outside at the interface between voltage sensor and plasma membrane.

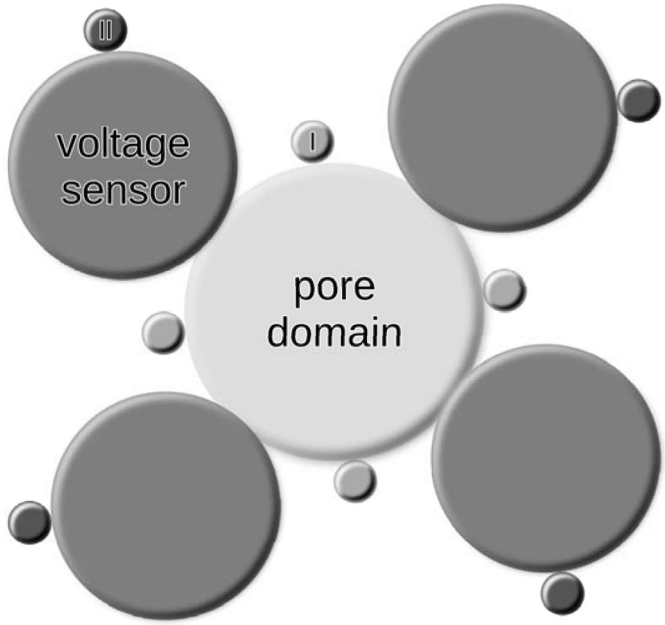

FIGURE 6. **Proposed positions of PIP_2 molecules around voltage-gated potassium channels.** The first PIP_2 binding site per subunit (*light gray*, labeled *I*) is located at the pore domain. We propose the second binding site (*dark gray*, labeled *II*) to be located at the voltage sensor.

We found that the absence of PIP_2 led to a higher structural flexibility of the pore domain and a distortion of the channel in both the open and closed conformation, suggested by conventional molecular dynamics simulations (Fig. 5). Thus, PIP_2 presence might result in a stabilization of the overall channel structure in both conformations. However, in the absence of the lipid, the structural stability of the closed conformation was decreased as suggested by the ~1 Å larger RMSD values compared with the structure in the presence of PIP_2. Consequently, the closed conformation might be structurally more stable in the absence of PIP_2. Hence, the thermodynamic equilibrium may be shifted to the closed state, increasing $V_{½}$ and thereby decreasing the open probability of the channel.

Thomas *et al.* (35) have previously shown that four amino acids within $K_v7.1$ helix S6, Lys-354, Lys-358, Arg-360, and Lys-362, directly interact with PIP_2. Based on double mutant analysis, they identified residues Lys-358 and Arg-360 as the most important ones. This is largely in agreement with our results, confirming the putative participation of Lys-354, Arg-360, and Lys-362 in PIP_2 interactions. Moreover, the importance of Arg-360 is underlined by the observation of completely abolished PIP_2 regulation when mutated. However, we could not find any significant participation of the residue Lys-358, because we observed no difference in PIP_2 sensitivity compared with WT. A possible explanation for this contradictory finding might be a weak interaction between PIP_2 and Lys-358 that can be functionally compensated by other amino acids interacting with PIP_2. However, if both residues are lost, compensation might not be possible anymore, increasing the impairment in PIP_2 regulation. However, these interpretations require further investigation. Furthermore, Zaydman *et al.* (59) included the same amino acids as in our study. However, comparison of both studies reveals discrepancies as to which amino acids participate in the interaction and which do not. However, it has to be considered that Zaydman *et al.* (59) did not analyze the influence of PIP_2 directly but rather hypothesized endogenous PIP_2 as the cause for loss of function of the mutant channels. Therefore, other influences cannot be excluded.

In summary, we showed that several $K_v7.1$ amino acids participate in the PIP_2 regulation of the cardiac I_{Ks} channel $K_v7.1$/KCNE1. These are located in both the S2-S3 and S4-S5 linker, as well as in the intracellular region of helix S6. Together with molecular dynamics simulations, our results suggested the existence of at least two specific PIP_2 binding sites per subunit. Disturbed binding caused by mutations of these amino acids may contribute to the manifestation of LQTS.

Acknowledgment—We thank G. N. Tseng (Virginia Commonwealth University, Richmond, VA) for providing the cysteine-free $K_v7.1$ clone.

REFERENCES

1. Sanguinetti, M. C., Curran, M. E., Zou, A., Shen, J., Spector, P. S., Atkinson, D. L., and Keating, M. T. (1996) Coassembly of KvLQT1 and minK (IsK) proteins to form cardiac I_{Ks} potassium channel. *Nature* **384,** 80–83
2. Demolombe, S., Franco, D., de Boer, P., Kuperschmidt, S., Roden, D., Pereon, Y., Jarry, A., Moorman, A. F., and Escande, D. (2001) Differential expression of KvLQT1 and its regulator IsK in mouse epithelia. *Am. J. Physiol. Cell. Physiol.* **280,** C359–C372
3. Barhanin, J., Lesage, F., Guillemare, E., Fink, M., Lazdunski, M., and Romey, G. (1996) KvLQT1 and lsK (minK) proteins associate to form the I_{Ks} cardiac potassium current. *Nature* **384,** 78–80
4. Schroeder, B. C., Waldegger, S., Fehr, S., Bleich, M., Warth, R., Greger, R., and Jentsch, T. J. (2000) A constitutively open potassium channel formed by KCNQ1 and KCNE3. *Nature* **403,** 196–199
5. Tinel, N., Diochot, S., Borsotto, M., Lazdunski, M., and Barhanin, J. (2000) KCNE2 confers background current characteristics to the cardiac KCNQ1 potassium channel. *EMBO J.* **19,** 6326–6330
6. Angelo, K., Jespersen, T., Grunnet, M., Nielsen, M. S., Klaerke, D. A., and Olesen, S.-P. (2002) KCNE5 induces time- and voltage-dependent modulation of the KCNQ1 current. *Biophys. J.* **83,** 1997–2006
7. Grunnet, M., Jespersen, T., Rasmussen, H. B., Ljungstrøm, T., Jorgensen, N. K., Olesen, S.-P., and Klaerke, D. A. (2002) KCNE4 is an inhibitory subunit to the KCNQ1 channel. *J. Physiol.* **542,** 119–130
8. Pusch, M. (1998) Increase of the single-channel conductance of KvLQT1 potassium channels induced by the association with minK. *Pflügers. Arch.* **437,** 172–174
9. Tristani-Firouzi, M., and Sanguinetti, M. C. (1998) Voltage-dependent inactivation of the human K^+ channel KvLQT1 is eliminated by association with minimal K^+ channel (minK) subunits. *J. Physiol.* **510,** 37–45
10. Tamargo, J., Caballero, R., Gómez, R., Valenzuela, C., and Delpón, E. (2004) Pharmacology of cardiac potassium channels. *Cardiovasc. Res.* **62,** 9–33
11. Nerbonne, J. M., and Kass, R. S. (2005) Molecular physiology of cardiac repolarization. *Physiol. Rev.* **85,** 1205–1253
12. Jespersen, T., Grunnet, M., and Olesen, S. (2005) The KCNQ1 potassium channel: from gene to physiological function. *Physiology* (*Bethesda*) **20,** 408–416
13. Jervell, A., and Lange-Nielsen, F. (1957) Congenital deaf-mutism, functional heart disease with prolongation of the Q-T interval and sudden death. *Am. Heart. J.* **54,** 59–68
14. Romano, C., Gemme, G., and Pongiglione, R. (1963) Rare cardiac arrhythmias of the pediatric age. I. repetitive paroxysmal tachycardia. *Minerva Pediatr.* **15,** 1155–1164
15. Fraser, G., Froggatt, P., and Murphy, T. (1964) Genetical aspects of the cardio-auditory syndrome of Jervell and Lange-Nielsen (congenital deaf-

ness and electrocardiographic abnormalities). *Ann. Hum. Genet.* **28,** 133–157
16. Ward, O. C. (1964) A new familial cardiac syndrome in children. *J. Ir. Med. Assoc.* **54,** 103–106
17. Moss, A. J., Schwartz, P. J., Crampton, R. S., Tzivoni, D., Locati, E. H., MacCluer, J., Hall, W. J., Weitkamp, L., Vincent, G. M., Garson, A., Jr., *et al.* (1991) The long QT syndrome. Prospective longitudinal study of 328 families. *Circulation* **84,** 1136–1144
18. Moss, A. J., Schwartz, P. J., Crampton, R. S., Locati, E., and Carleen, E. (1985) The long QT syndrome: a prospective international study. *Circulation* **71,** 17–21
19. Pfaffinger, P. (1988) Muscarine and t-LHRH suppress M-current by activating an IAP-insensitive G-protein. *J. Neurosci.* **8,** 3343–3353
20. Lopez, H. S., and Adams, P. R. (1989) A G protein mediates the inhibition of the voltage-dependent potassium M current by muscarine, LHRH, substance P and UTP in bullfrog sympathetic neurons. *Eur. J. Neurosci.* **1,** 529–542
21. Selyanko, A. A., Hadley, J. K., Wood, I. C., Abogadie, F. C., Jentsch, T. J., and Brown, D. A. (2000) Inhibition of KCNQ1–4 potassium channels expressed in mammalian cells via M_1 muscarinic acetylcholine receptors. *J. Physiol.* **522,** 349–355
22. Delmas, P., and Brown, D. (2005) Pathways modulating neural KCNQ/M (Kv7) potassium channels. *Nat. Rev. Neurosci.* **6,** 850–862
23. Berridge, M. (1984) Inositol trisphosphate and diacylglycerol as second messengers. *Biochem. J.* **220,** 345–360
24. Suh, B. C., and Hille, B. (2002) Recovery from muscarinic modulation of M current channels requires phosphatidylinositol 4,5-bisphosphate synthesis. *Neuron* **35,** 507–520
25. Zhang, H., Craciun, L. C., Mirshahi, T., Rohács, T., Lopes, C. M., Jin, T., and Logothetis, D. E. (2003) PIP_2 activates KCNQ channels, and its hydrolysis underlies receptor-mediated inhibition of M currents. *Neuron* **37,** 963–975
26. Huijbregts, R. P., Topalof, L., and Bankaitis, V. A. (2000) Lipid metabolism and regulation of membrane trafficking. *Traffic* **1,** 195–202
27. Martin, T. (2001) $PI(4,5)P_2$ regulation of surface membrane traffic. *Curr. Opin. Cell Biol.* **13,** 493–499
28. Nebl, T., Oh, S. W., and Luna, E. J. (2000) Membrane cytoskeleton: PIP_2 pulls the strings. *Curr. Biol.* **10,** R351–R354
29. Sechi, A. S., and Wehland, J. (2000) The actin cytoskeleton and plasma membrane connection: $PtdIns(4,5)P_2$ influences cytoskeletal protein activity at the plasma membrane. *J. Cell Sci.* **113,** 3685–3695
30. Hilgemann, D. W., Feng, S., and Nasuhoglu, C. (2001) The complex and intriguing lives of PIP_2 with ion channels and transporters. *Sci. STKE* 2001, re19
31. Seebohm, G., Wrobel, E., Pusch, M., Dicks, M., Terhag, J., Matschke, V., Rothenberg, I., Ursu, O., Hertel, F., Pott, L., Lang, F., Schulze-Bahr, E., Hollmann, M., Stoll, R., and Strutz-Seebohm, N. (2014) Structural basis of $PI(4,5)P_2$-dependent regulation of GluA1 by phosphatidylinositol-5-phosphate 4-kinase, type II, alpha (PIP5K2A). *Pflügers Arch.*, in press
32. Chuang, H. H., Prescott, E. D., Kong, H., Shields, S., Jordt, S. E., Basbaum, A. I., Chao, M. V., and Julius, D. (2001) Bradykinin and nerve growth factor release the capsaicin receptor from $PtdIns(4,5)P_2$-mediated inhibition. *Nature* **411,** 957–962
33. Huang, C. L., Feng, S., and Hilgemann, D. W. (1998) Direct activation of inward rectifier potassium channels by PIP_2 and its stabilization by Gbetagamma. *Nature* **391,** 803–806
34. Loussouarn, G., Park, K.-H., Bellocq, C., Baró, I., Charpentier, F., and Escande D. (2003) Phosphatidylinositol-4,5-bisphosphate, PIP_2, controls KCNQ1/KCNE1 voltage-gated potassium channels: a functional homology between voltage-gated and inward rectifier K^+ channels. *EMBO J.* **22,** 5412–5421
35. Thomas, A. M., Harmer, S. C., Khambra, T., and Tinker, A. (2011) Characterisation of a binding site for anionic phospholipids on KCNQ1. *J. Biol. Chem.* **286,** 2088–2100
36. Seebohm, G., Strutz-Seebohm, N., Baltaev, R., Korniychuk, G., Knirsch, M., Engel, J., and Lang, F. (2005) Regulation of KCNQ4 potassium channel prepulse dependence and current amplitude by SGK1 in *Xenopus* oocytes. *Cell. Physiol. Biochem.* **16,** 255–262
37. Xu, X., Jiang, M., Hsu, K.-L., Zhang, M., and Tseng, G.-N. (2008) KCNQ1 and KCNE1 in the I_{Ks} channel complex make state-dependent contacts in their extracellular domains. *J. Gen. Physiol.* **131,** 589–603
38. Kang, C., Tian, C., Sönnichsen, F. D., Smith, J. A., Meiler, J., George, A. L., Jr., Vanoye, C. G., Kim, H. J., and Sanders, C. R. (2008) Structure of KCNE1 and implications for how it modulates the KCNQ1 potassium channel. *Biochemistry* **47,** 7999–8006
39. Strutz-Seebohm, N., Pusch, M., Wolf, S., Stoll, R., Tapken, D., Gerwert, K., Attali, B., and Seebohm, G. (2011) Structural basis of slow activation gating in the cardiac I_{Ks} channel complex. *Cell. Physiol. Biochem.* **27,** 443–452
40. Wrobel, E., Tapken, D., and Seebohm, G. (2012) The KCNE Tango: how KCNE1 interacts with Kv7.1. *Front. Pharmacol.* **3,** 142
41. Hansen, S. B., Tao, X., and MacKinnon, R. (2011) Structural basis of PIP_2 activation of the classical inward rectifier K^+ channel Kir2.2. *Nature* **477,** 495–498
42. Whorton, M. R., and MacKinnon, R. (2011) Crystal structure of the mammalian GIRK2 K^+ channel and gating regulation by G proteins, PIP_2, and sodium. *Cell.* **147,** 199–208
43. Seebohm, G., Lerche, C., Busch, A. E., and Bachmann, A. (2001) Dependence of I_{Ks} biophysical properties on the expression system. *Pflügers Arch.* **442,** 891–895
44. Fan, Z., and Makielski, J. C. (1997) Anionic phospholipids activate ATP-sensitive potassium channels. *J. Biol. Chem.* **272,** 5388–5395
45. Zhang, H., He, C., Yan, X., Mirshahi, T., and Logothetis, D. E. (1999) Activation of inwardly rectifying K^+ channels by distinct $PtdIns(4,5)P_2$ interactions. *Nat. Cell Biol.* **1,** 183–188
46. Shyng, S. L., Cukras, C. A., Harwood, J., and Nichols, C. G. (2000) Structural determinants of PIP_2 regulation of inward rectifier K_{ATP} channels. *J. Gen. Physiol.* **116,** 599–608
47. Lopes, C. M., Zhang, H., Rohacs, T., Jin, T., Yang, J., and Logothetis, D. E. (2002) Alterations in conserved Kir channel-PIP_2 interactions underlie channelopathies. *Neuron.* **34,** 933–944
48. Thomas, A. M., Brown, S. G., Leaney, J. L., and Tinker, A. (2006) Differential phosphoinositide binding to components of the G protein-gated K^+ channel. *J. Membr. Biol.* **211,** 43–53
49. Hernandez, C. C., Zaika, O., and Shapiro, M. S. (2008) A carboxy-terminal inter-helix linker as the site of phosphatidylinositol 4,5-bisphosphate action on Kv7 (M-type) K^+ channels. *J. Gen. Physiol.* **132,** 361–381
50. Park, K. H., Piron, J., Dahimene, S., Mérot, J., Baró, I., Escande, D., and Loussouarn, G. (2005) Impaired KCNQ1-KCNE1 and phosphatidylinositol-4,5-bisphosphate interaction underlies the long QT syndrome. *Circ. Res.* **96,** 730–739
51. Donger, C., Denjoy, I., Berthet, M., Neyroud, N., Cruaud, C., Bennaceur, M., Chivoret, G., Schwartz, K., Coumel, P., and Guicheney, P. (1997) KVLQT1 C-terminal missense mutation causes a forme fruste long-QT syndrome. *Circulation* **96,** 2778–2781
52. Chouabe, C., Neyroud, N., Richard, P., Denjoy, I., Hainque, B., Romey, G., Drici, M. D., Guicheney, P., and Barhanin, J. (2000) Novel mutations in KvLQT1 that affect I_{Ks} activation through interactions with Isk. *Cardiovasc. Res.* **45,** 971–980
53. Kubota, T., Shimizu, W., Kamakura, S., and Horie, M. (2000) Hypokalemia-induced long QT syndrome with an underlying novel missense mutation in S4-S5 linker of KCNQ1. *J. Cardiovasc. Electrophysiol.* **11,** 1048–1054
54. Napolitano, C., Priori, S. G., Schwartz, P. J., Bloise, R., Ronchetti, E., Nastoli, J., Bottelli, G., Cerrone, M., and Leonardi, S. (2005) Genetic testing in the long QT syndrome: development and validation of an efficient approach to genotyping in clinical practice. *JAMA* **294,** 2975–2980
55. Millat, G., Chevalier, P., Restier-Miron, L., Da Costa, A., Bouvagnet, P., Kugener, B., Fayol, L., Gonzàlez Armengod, C., Oddou, B., Chanavat, V., Froidefond, E., Perraudin, R., Rousson, R., and Rodriguez-Lafrasse, C. (2006) Spectrum of pathogenic mutations and associated polymorphisms in a cohort of 44 unrelated patients with long QT syndrome. *Clin. Genet.* **70,** 214–227
56. Kapplinger, J. D., Tester, D. J., Salisbury, B. A., Carr, J. L., Harris-Kerr, C., Pollevick, G. D., Wilde, A. A., and Ackerman, M. J. (2009) Spectrum and

prevalence of mutations from the first 2,500 consecutive unrelated patients referred for the FAMILION long QT syndrome genetic test. *Heart Rhythm.* **6,** 1297–1303

57. Yang, T., Chung, S.-K., Zhang, W., Mullins, J. G., McCulley, C. H., Crawford, J., MacCormick, J., Eddy, C.-A., Shelling, A. N., French, J. K., Yang, P., Skinner, J. R., Roden, D. M., and Rees, M. I. (2009) Biophysical properties of 9 KCNQ1 mutations associated with long-QT syndrome. *Circ. Arrhythm. Electrophysiol.* **2,** 417–426
58. Kanovsky, J., Novotny, T., Kadlecova, J., and Gaillyova, R. (2010) A new homozygous mutation of the KCNQ1 gene associated with both Romano-Ward and incomplete Jervell Lange-Nielsen syndromes in two sisters. *Heart Rhythm.* **7,** 531–533
59. Zaydman, M. A., Silva, J. R., Delaloye, K., Li, Y., Liang, H., Larsson, H. P., Shi, J., and Cui, J. (2013) Kv7.1 ion channels require a lipid to couple voltage sensing to pore opening. *Proc. Natl. Acad. Sci. U.S.A.* **110,** 13180–13185